Size-dependent enhancement of nonlinear optical susceptibilities due to confined excitons in CuBr nanocrystals

Yingli Li, Masaki Takata,* and Arao Nakamura
Department of Applied Physics, and Center for Integrated Research in Science and Engineering, Nagoya University, Chikusa-ku, Nagoya 464-8603 Japan
(Received 12 September 1997)

We have investigated the third-order nonlinearity on resonance with the confined exciton level in CuBr nanocrystals with radii in the range 2.7–42 nm embedded in glass by means of degenerate four-wave mixing, time-resolved luminescence, and resonant luminescence measurements. The third-order optical susceptibility $\chi^{(3)}$ exhibits resonant behaviors at Z_{12} and Z_3 excitons, which are weakly confined in nanocrystals. The figure of merit $|\chi^{(3)}|/\alpha$ increases with increasing radius R in the whole range studied here. We have measured homogeneous widths and lifetimes of Z_{12} excitons and obtained size dependences of those relaxation parameters. Assuming a two-level atomic model for the confined exciton, we have deduced the size dependence of the oscillator strength of Z_{12} excitons from the measured lifetimes, homogeneous widths, and $\chi^{(3)}$. The oscillator strength exhibits the $R^{2.0}$ dependence in the whole range studied here, which reveals the giant oscillator strength effect on the confined exciton that is coherently generated in the nanocrystal. The oscillator strength per nanocrystal is enhanced by a factor 1.7×10^3 for $R=42$ nm compared to that of bulk excitons. We also discuss the derivation of $\chi^{(3)}$ in the stationary regime from the $\chi^{(3)}$ in the transient regime where the nonlinear time response shows a multiexponential decay. [S0163-1829(98)05215-1]

I. INTRODUCTION

The potential need for highly efficient optical devices stimulates the exploration for different materials with high optical nonlinearities. The progress in fabrication techniques of nano-structured semiconductors has enabled us to study nonlinear optical properties in mesoscopic systems. Optical nonlinearities especially in GaAs-based semiconductor quantum-well structures have been extensively studied and it has been known that quasi-two-dimensional excitons give rise to the strong nonlinear response in the vicinity of the band gap.[1] Since the pioneering work on CdS_xSe_{1-x} nanocrystals,[2] a great deal of effort has been devoted to fabricating various kinds of nanocrystals and elucidating the origin of nonlinearity in nanocrystals.

When the crystallite size is reduced to the order of an exciton Bohr radius a_B, quantum size effects appear and drastic changes of optical properties are expected. The quantum confinement effects in semiconductor nanocrystals can be classified into two regimes, i.e., strong- and weak-confinement regimes, according to the ratio of nanocrystal radius R to a_B.[3–5] Nonlinear optical properties in nanocrystals have been also investigated for the corresponding confinement regimes. In the strong-confinement regime, the photoexcited electron and hole are individually confined. Theoretical and experimental works have revealed that the state-filling effect accounts for the nonlinearity in this regime.[6,7] The size dependence of the third-order susceptibility $\chi^{(3)}$ also has been studied, but the results are inconsistent; a larger nonlinear susceptibility for a larger size has been found for CdS_xSe_{1-x} nanocrystals by the saturation spectroscopy[8,9] and degenerate four-wave mixing (DFWM) measurements,[10] while Roussignol *et al.* have shown that the larger $\chi^{(3)}$ values are obtained with decreasing sizes.[7]

In the weak-confinement regime, the Coulomb interaction between the electron and hole yields an exciton and the exciton is confined as a quasiparticle. The nonlinearity arises from the exciton-exciton interaction, which results in the deviation of harmonicity of the bosonlike exciton within the nanocrystal, and the size enhancement of nonlinear susceptibility has been investigated theoretically[11–14] and experimentally.[15–19] The theoretical studies have shown that the confinement of the excitonic envelope wave function due to the infinite barrier potential gives rise to the enhancement of the oscillator strength for an exciton within the nanocrystal by a factor of R^3/a_B^3 and hence $\chi^{(3)}$ depends on the crystallite size.[11,12] Such a giant oscillator strength effect has been confirmed for CuCl nanocrystals; the radiative decay rate of confined excitons is proportional to $R^{2.1}$ for the glass matrix[20] and R^3 for the NaCl crystal matrix.[21] The validity of the size-enhancement effect is limited by the long-wavelength approximation and a nonlocal theory applicable to the mesoscopic system larger than the wavelength has been developed.[14] The important role of the giant oscillator strength effect in the size enhancement of nonlinearity has been experimentally shown for CuCl nanocrystals.[17] As the quantum-confined exciton system can be modeled as a two-level atomic system, the imaginary part of $\chi^{(3)}$ on resonance in the low-density regime is given by

$$\mathrm{Im}\ \chi^{(3)}=\left(\frac{e^2}{2m_0\omega}\right)^2 \hbar N f_x^2 \frac{T_1}{\Gamma_h^2}, \tag{1}$$

where T_1 and Γ_h are the longitudinal relaxation time and homogeneous width, respectively, and f_x and N are the oscillator strength and the number density of nanocrystals, respectively. The detailed study measuring the susceptibility on resonance and the relaxation parameters T_1 and Γ_h revealed that the oscillator strength per nanocrystal exhibits an intriguing feature in the size range $R=1.5-8.0$ nm at 80 K,

i.e., $f_x \propto R^{2.2}$ at 1.9–4.0 nm, and subsequently decreases for $R \geqslant 5.0$ nm.[17] Although the $R^{2.2}$ dependence of f_x indicates the giant oscillator strength of coherently generated excitons in nanocrystals, the saturation and decrease of f_x for larger sizes cannot be explained by the two-level atomic model. This result suggests that there exist additional contributions, such as higher excited states and a two-exciton state, to the nonlinearity in larger nanocrystals.

In CuBr, the exciton Bohr radius is 1.25 nm, which is roughly twice that of CuCl, and one can investigate confinement effects and size dependence of $\chi^{(3)}$ over a wide range of crystallite sizes from the strong-confinement regime to the weak-confinement regime.[22] The lowest exciton state in CuBr is the Z_{12} exciton consisting of light and heavy holes in the Γ_8 band, while that of CuCl is the Z_3 exciton coming from the Γ_7 band. In addition, a k-linear term in the Γ_8 band is not negligible in CuBr and thus the Z_{12} exciton has a multicomponent character. Therefore, we can also investigate an effect of multicomponent exciton states on the giant oscillator strength effect using CuBr nanocrystals.

In this paper we report a detailed study of the size-dependent optical nonlinearity in CuBr nanocrystals over a wide range of sizes. We used samples of CuBr nanocrystals embedded in borosilicate glasses with radii in the range $2.7-42$ nm. The third-order nonlinear susceptibility $\chi^{(3)}$ around the resonance of Z_3 and Z_{12} excitons was measured by degenerate four-wave mixing with a two-beam configuration. The lifetimes and the homogeneous widths of Z_{12} excitons for various crystallite sizes were measured by the time-resolved luminescence and the resonant luminescence experiments, respectively. The figure of merit $|\chi^{(3)}|/\alpha$ measured at the resonance of Z_{12} excitons is size dependent and the experimental results were analyzed by taking into account a two-level model. From the measured size dependences of $|\chi^{(3)}|$, T_1, and Γ_h, the size dependence of the oscillator strength f_x per nanocrystal is derived: $f_x \propto R^{2.0}$ when 2.7 nm $\leqslant R \leqslant 42$ nm, without showing a saturation behavior of f_x in the size range studied here. We also discuss $\chi^{(3)}$ values in the stationary regime and the transient regime where the nonlinear time response shows a multiexponential decay and point out that the stationary susceptibility is a nonlinear parameter characterizing uniquely the nonlinearity of materials. The paper is organized as follows. In Sec. II the sample preparation and the experimental methods are described. The experimental results and the derived size dependence of the oscillator strength are presented in Sec. III. Section IV is devoted to a discussion and we summarize our conclusion in Sec. V.

II. EXPERIMENT

A. Preparation of CuBr nanocrystals

Samples of CuBr nanocrystals embedded in a glass matrix were obtained by the double heat-treatment procedure of borosilicate glasses doped with CuBr.[20,23] The glasses were heat treated at temperatures of 450–600 °C for duration of 30 min to several days to obtain CuBr nanocrystals with various sizes. Samples for optical measurements were prepared by polishing to thickness of about 200 μm.

The mean radii of CuBr nanocrystals were determined by the x-ray diffraction (XRD) method using a synchrotron radiation (SR) light source at Photon Factory in Tsukuba and a conventional x-ray source. The high-intensity SR light and the two-dimensional imaging plate made the measurement of wide angle diffraction possible to finish within 1 h with a satisfactory signal-to-noise ratio.

The mean radius of nanocrystals is estimated from the broadening of the diffraction pattern by using the Scherrer formula

$$R = \frac{2}{3}\frac{0.9\lambda}{w\cos\theta}, \tag{2}$$

where λ is the wavelength of the x-ray radiation and θ and w are the diffraction angle and the full width at half maximum of the diffraction peak, respectively. A careful least-squares profile fitting was applied to separate the diffraction pattern of CuBr nanocrystals from that of the glass background. The diffraction profiles of (220) and (311) were fitted to Gaussian functions with the same broadening parameter w. The parameter w was determined within a fitting error of 10%. In order to confirm the reliability of the radius estimated from Eq. (2), we further performed a small-angle x-ray scattering (SAXS) experiment on two samples.

B. Measurements of $\chi^{(3)}$, T_1, and Γ_h

The absolute values of $\chi^{(3)}$ were measured by degenerate four-wave mixing with the two-beam configuration.[23] We used a XeCl excimer-laser pumped dye [2-(4-biphenylyl)-6-phenylbenzoxazol-1,3] laser with a laser pulse width of 20 ns operating at a repetition rate of 10 Hz. The two laser beams with a crossing angle of about 1° were focused onto the sample. The spatially separated diffraction signal was then collected by a photomultiplier and the signal was averaged by a boxcar integrator. The pumping laser intensity was reduced to a level that is low enough to ensure that the detected nonlinearity is due to the third-order nonlinear polarizability.

A value of $|\chi^{(3)}|$ in esu was calculated using the formula

$$|\chi^{(3)}| = \frac{n^2 c}{32\pi^3}\frac{\alpha\lambda}{(1-T)\sqrt{T}}\sqrt{\frac{\eta}{I_0}}, \tag{3}$$

where c is the velocity in vacuum and n is the refractive index of glass (taken as 1.5 for the glass used here). α and T are the absorption coefficient and transmittance at wavelength λ, respectively, and I_0 is the intensity of the laser beam incident on the surface of sample. The diffraction efficiency η is defined as a ratio of the diffraction signal intensity to I_0. Equation (3) is valid only for the cw case where the pulse duration t_p of pumping light is much longer than the nonlinear response time T_1 involved. In the transient case, i.e., $t_p \ll T_1$, one must use the following equation to obtain a $|\chi^{(3)}|$ value that can be compared with the $|\chi^{(3)}|$ value for the cw case:[24]

$$|\chi^{(3)}| = \frac{n^2 c}{32\pi^3}\frac{\alpha\lambda}{(1-T)\sqrt{T}}\sqrt{\frac{\eta_{obs}}{I_0}}\beta\frac{T_1}{t_p}. \tag{4}$$

Here β is a dimensionless numerical constant, dependent on the temporal shape of laser pulse. If the factor of $\beta T_1/t_p$ is not taken into account [i.e., Eq. (3)], the estimated $\chi^{(3)}$ value from the measured η_{obs} under the condition of $t_p \ll T_1$ is

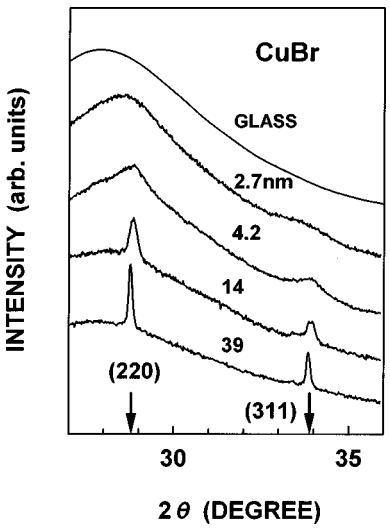

FIG. 1. X-ray-diffraction patterns of CuBr nanocrystals embedded in glass for different crystallite radii and an untreated base-glass sample. Two vertical arrows indicate the positions of diffraction peaks arising from (220) and (311) planes in bulk CuBr with the zinc-blende structure. The mean radii obtained by using the Scherrer formula are shown in the figure.

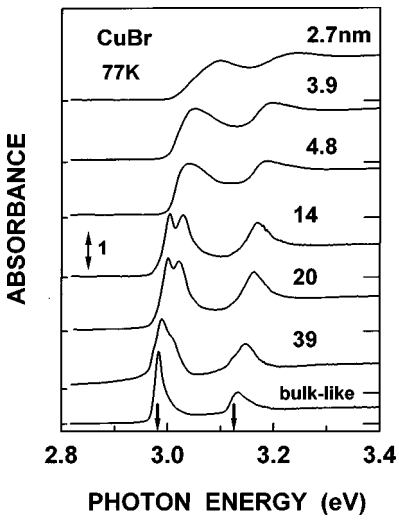

FIG. 2. Absorption spectra of CuBr nanocrystals at 77 K. The vertical arrows indicate absorption energies of the bulk Z_{12} and Z_3 excitons.

always smaller than that measured under the cw excitation condition ($t_p \gg T_1$). Such a $\chi^{(3)}$ value can be only referred to as an effective $\chi^{(3)}$ in the transient regime because it is dependent on the ratio T_1/t_p. We will discuss a formula to estimate a $|\chi^{(3)}|$ value for the case where the nonlinear time response exhibits a multicomponent decay in Sec. IV.

The longitudinal relaxation time of Z_{12} excitons was determined from the luminescence decay kinetics measured by utilizing a picosecond pulse laser and a time-correlated single photon counting system. The excitation light of 375 nm was generated by the sum frequency of 1.06-μm fundamental light and 580-nm dye laser output of a synchronously mode-locked dye laser pumped by a mode-locked Nd:YAG laser (532 nm) (where YAG denotes yttrium aluminum garnet). The pulse width and the repetition rate were about 10 ps and 0.8−4 MHz, respectively. The deconvolution of the luminescence decay curve with the apparatus response of the laser pulse yielded a time resolution of about 20 ps. We used resonant luminescence measurements to obtain the homogeneous width of the Z_{12} exciton band. Resonant luminescence was collected and focused onto a double monochromator with a spectral resolution of 0.4 meV.

III. RESULTS

Figure 1 shows the XRD patterns of CuBr-doped glass samples after the heat treatment and a base-glass sample without the heat treatment. Distinguishable diffraction peaks that are superimposed on the broad halo pattern due to the matrix glass are seen at 28.78° and 33.88° for all the heat-treated samples. Two vertical arrows indicate the diffraction angles from (220) and (311) planes in the CuBr bulk crystal with the zinc-blende structure. The agreement of the observed peak positions with that of the bulk crystal is satisfactory, which indicates that CuBr nanocrystals with the zinc-blende structure are obtained. The diffraction profiles due to (220) and (311) planes were analyzed using Eq. (2) and the obtained radii are shown in Fig. 1. The two samples ($R=4.2$ and 14 nm) were also set to SAXS measurements. The mean radii obtained by the SAXS method turned out to be 4.2 nm and 15 nm, respectively. The radii determined by both methods agree well within the experimental error of 10%.

Absorption spectra of CuBr nanocrystals with various radii are shown in Fig. 2. At the bottom of the figure a spectrum for the bulklike crystal is shown. The vertical arrows indicate the Z_{12} and Z_3 exciton absorption peaks from the lower-energy side in the bulk CuBr crystal. Both the absorption bands exhibit a blueshift with decreasing radii. The size-dependent behaviors of the absorption spectra can be classified into two regimes according to R. In the size range $2.7 \leqslant R \leqslant 5.0$ nm, both the Z_{12} and Z_3 bands are shifted to the higher-energy side by 50−120 meV with decreasing radii. In the size range $5.0 \leqslant R \leqslant 39$ nm, the absorption band due to Z_{12} excitons splits into two peaks with an energy separation of about 25 meV. The center of mass of the Z_{12} band shifts to the higher-energy sides by 23−50 meV upon a decrease of size. The splitting of the Z_{12} band is not due to a size distribution because we cannot observe any obvious structure in the Z_3 band. It may be attributed to the splitting of light- and heavy-hole excitons.

Figure 3 shows the excitation intensity dependence of diffraction efficiency in DFWM experiments for CuBr nanocrystals with $R=4.0$ nm at 77 K. η was measured at the absorption peak of Z_{12} excitons. The value measured exhibits the square dependence on the excitation intensity as shown by the dashed line up to the excitation level of 20 kW/cm^2 and starts to deviate from this dependence at higher excitation intensities. In this study the DFWM experiments were performed at a level low enough to show the square dependence that indicates that the third-order nonlinearity is involved.

Figure 4 depicts the photon energy dependence of the absolute value of $\chi^{(3)}$ measured at 77 K for CuBr nanocrystals with various radii. The magnitude of $|\chi^{(3)}|$ shown by open circles is greatly enhanced in the vicinity of the absorp-

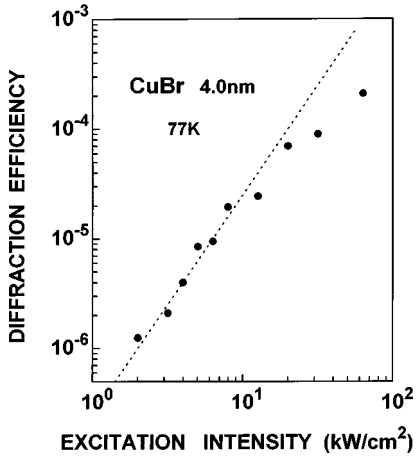

FIG. 3. Excitation intensity dependence of diffraction efficiency in DFWM for CuBr nanocrystals with $R=4.0$ nm. The dashed line indicates the square dependence.

tion peaks of Z_{12} and Z_3 excitons, indicating the resonant enhancement with the confined excitons. Note that $|\chi^{(3)}|$ is shown on a logarithmic scale and the width of $|\chi^{(3)}|$ is considerably narrower than the absorption bandwidth. For $R=25$ nm, $|\chi^{(3)}|$ exhibits clearly two maxima, while in the absorption spectrum one peak and a shoulder are seen. The sharp resonant behavior of $|\chi^{(3)}|$ is consistent with the fact that the higher-order interaction between light and matter is involved in the third-order nonlinear process compared to the absorption process. The value of $|\chi^{(3)}|$ at the resonance of Z_{12} excitons is strongly sample dependent and ranges from 8.3×10^{-9} esu to 2.6×10^{-7} esu for the samples shown in Fig. 4, which implies that $|\chi^{(3)}|$ is size dependent.

In order to obtain the crystallite size dependence of the third-order susceptibility, we must take into account the difference in the number density of nanocrystals contained in the samples under measurements. Since the absorption coefficient is proportional to the number of nanocrystals in the sample, we use a value of $|\chi^{(3)}|/\alpha$ for the comparison between the different sizes. The R dependence of $|\chi^{(3)}|/\alpha$ measured at the absorption peak of Z_{12} excitons is shown in Fig. 5. The data show a general trend of increasing $|\chi^{(3)}|/\alpha$ values upon an increase of the radius and the values range from 8.0×10^{-11} to 1.1×10^{-9} esu cm for $R=2.7-42$ nm. When we apply a least-squares fit, a size dependence of $R^{0.4}$ is obtained. There is, however, a noticeable scattering in the data, which implies that the $|\chi^{(3)}|$ is dependent on some parameters other than the size.

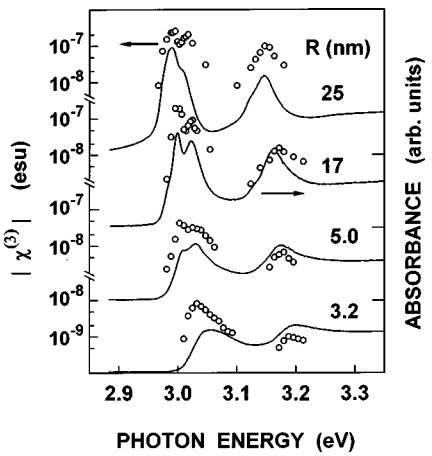

FIG. 4. Photon energy dependence of $|\chi^{(3)}|$ for CuBr nanocrystals with different mean radii. Open circles and solid curves illustrate $|\chi^{(3)}|$ and the absorption spectra, respectively.

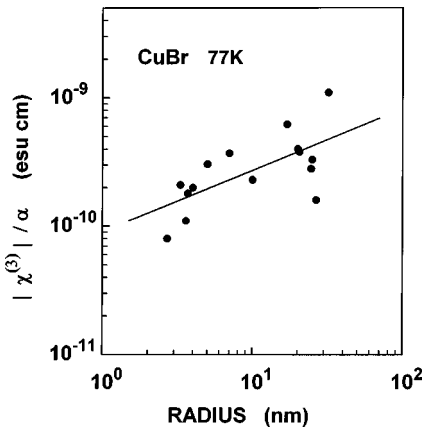

FIG. 5. $|\chi^{(3)}|/\alpha$ as a function of crystallite radii for CuBr nanocrystals at 77 K. The straight line indicates the result of a least-squares fit, which is the $R^{0.4}$ dependence.

The laser spectral width used in this study (0.02 meV) is much narrower than the spectral width of the Z_{12} absorption band that is inhomogeneously broadened because of the size distribution. Thus, in our experiments we excite selectively the nanocrystals in which the pumping light is resonant with the Z_{12} exciton level with Γ_h. The measured diffraction efficiency gives a $|\chi^{(3)}|$ value for the nanocrystals with a certain size within the size distribution. In this case $N_p f_x$ is proportional to $\alpha\Gamma_h$, where N_p is the number density of nanocrystals selectively excited and α is the absorption coefficient at the laser frequency.[7] Therefore, Eq. (1) is rewritten as

$$\mathrm{Im}\ \chi^{(3)}/\alpha \propto f_x \frac{T_1}{\Gamma_h}. \tag{5}$$

As the $|\chi^{(3)}|$ value at the resonance peak is approximately equal to $\mathrm{Im}\chi^{(3)}$, the observed dependence of $|\chi^{(3)}|/\alpha$ shown in Fig. 5 suggests that $f_x(T_1/\Gamma_h)$ is dependent on the samples. Consequently, we further need to measure size dependences of T_1 and Γ_h in order to investigate the origin of the size-dependent behavior of $|\chi^{(3)}|/\alpha$.

Figure 6 shows the decay curve of the luminescence due to Z_{12} excitons for the sample with $R=4.0$ nm at 77 K. As shown in the inset, the decay curve on the time scale up to 500 ns exhibits a multicomponent decay. As there exist a size distribution of nanocrystals in the sample, the emission band consists of contributions from different nanocrystals, which results in the distribution of decay constants. Assuming the three exponential decay components

$$I(t)=a\ \exp\left(-\frac{t}{\tau_1}\right)+b\ \exp\left(-\frac{t}{\tau_2}\right)+c\ \exp\left(-\frac{t}{\tau_3}\right), \tag{6}$$

an effective lifetime T_1^* is defined as

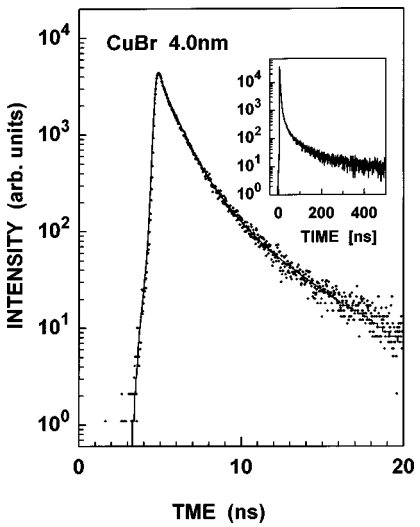

FIG. 6. Decay curves of luminescence due to Z_{12} excitons in CuBr nanocrystals with $R=4.0$ nm at 77 K. The solid curve shows the fitted curve with the three-exponential decay. The inset displays the decay on an extended scale.

$$T_1^*=\frac{a\tau_1+b\tau_2+c\tau_3}{a+b+c}. \tag{7}$$

Fitting Eq. (6) to the decay curve in Fig. 6, we obtained 2.0, 30, and 400 ns for τ_1, τ_2, and τ_3 and the coefficients a, b and c were 1, 0.02, and 0.001, respectively. T_1^* turns out to be 2.9 ns, which is dominated by the fast decay component. Figure 7 shows the R dependence of T_1^* at 77 K. T_1^* decreases from 2 ns to 30 ps with increasing R for $2.7-42$ nm. The least-squares fit yields the $R^{-1.5}$ dependence, but the data are scattered around this dependence. As the measured decay time is governed by the nonradiative recombination process as well as the radiative process, T_1^* depends on the samples.

The size dependence of homogeneous width was investigated by resonant luminescence spectroscopy. Figure 8 shows the emission spectra for different radii at 77 K. All the spectra were obtained under the same excitation level as in

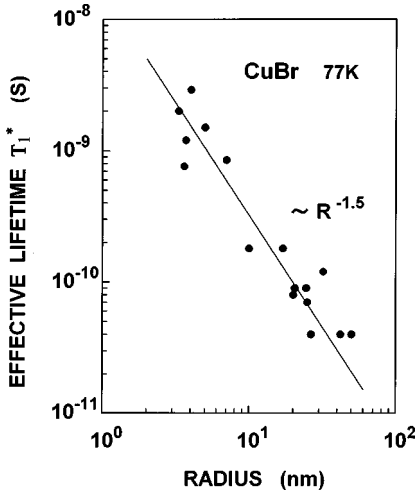

FIG. 7. Crystallite radius dependence of the effective lifetime T_1^* in CuBr nanocrystals at 77 K. The solid line is the result of a least-squares fit indicating the $R^{-1.5}$ dependence.

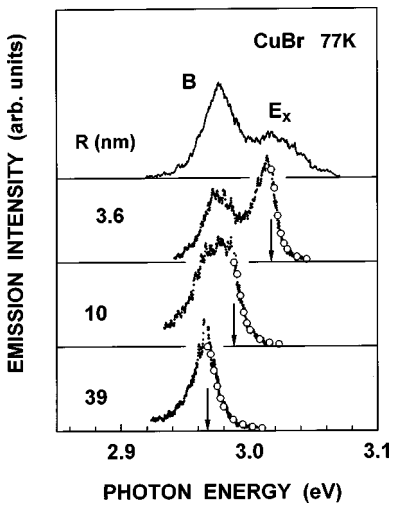

FIG. 8. Resonant luminescence spectra of CuBr nanocrystals with different radii at 77 K. The uppermost spectrum shows the luminescence spectrum for $R=3.6$ nm under the interband excitation. The two emission bands are due to excitons (E_x) and biexcitons (B), respectively. Open circles indicate Lorentzian fittings.

the DFWM experiments. The uppermost spectrum shows the emission spectrum measured by interband excitation for the sample with $R=3.6$ nm. The two emission bands are assigned to Z_{12} excitons (E_x) and biexcitons (B). When we changed the laser wavelength as indicated by vertical arrows, we observed the considerably narrow luminescence spectrum in the higher-energy side of excitation energy. The spectral shape in the higher-energy side can be well fitted to the Lorentzian function and we attribute this spectrum to the resonant luminescence from the size-selected nanocrystals within the size distribution. When the inhomogeneous width is much larger than the homogeneous width, half of the half width at half maximum of the resonant luminescence band corresponds to Γ_h. Γ_h was found to be independent of the excitation intensity between 10 and 100 kW/cm^2. In Fig. 8 the widths are 2.5, 3.1, and 4.0 meV for $R=3.6$, 10, and 39 nm, respectively. In order to investigate the mechanism that determines Γ_h, we measured resonant luminescence for the sample with $R=3.6$ nm changing temperatures between 8 and 170 K. As Γ_h is proportional to the temperature in the range $8-50$ K, Γ_h is mainly governed by the accoustic-phonon scattering via piezoelectric coupling and deformation potential coupling.

The radius dependence of Γ_h at 77 K is shown in Fig. 9. Γ_h is weakly dependent on the radius and exhibits the $R^{0.1}$ dependence. The width varies from 2.5 meV to 4.0 meV when R is increased from 2.7 nm to 39 nm. The values of Γ_h are in agreement with the results that were obtained from the resonant luminescence spectroscopy[25] and persistent hole-burning spectroscopy[26] for CuCl nanocrystals embedded in NaCl crystals. We have also done persistent hole-burning experiments at the excitation levels of ~ 100 kW/cm^2 and obtained similar results.[27]

Now we elucidate the size dependence of the oscillator strength of the confined Z_{12} exciton, using the size dependences of $|\chi^{(3)}|/\alpha$, Γ_h, and T_1^*. The size dependence of $|\chi^{(3)}|\Gamma_h/\alpha T_1^*$, which is proportional to f_x, is plotted in Fig. 10. In the size range $2.7\leqslant R\leqslant 42$ nm, $\chi^{(3)}\Gamma_h/\alpha T_1^*$ exhibits

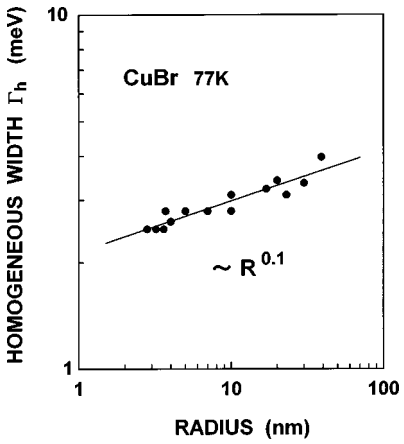

FIG. 9. Crystallite radius dependence of the homogeneous width of the Z_{12} exciton band in CuBr nanocrystals at 77 K. The solid line is the result of a least-squares fit that indicates the $R^{0.1}$ dependence.

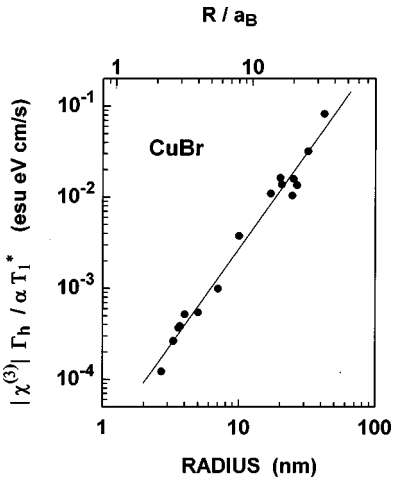

FIG. 10. Crystallite radius dependence of $|\chi^{(3)}|\Gamma_h/\alpha T_1^*$ being proportional to the oscillator strength of Z_{12} excitons in CuBr nanocrystals. The solid line is the result of a least-squares fit that indicates the $R^{2.0}$ dependence.

an $R^{2.0}$ dependence, indicating an enhancement of more than two orders of magnitude. This dependence is in good agreement with that observed for CuCl nanocrystals, which is $R^{2.1}$.[17]

IV. DISCUSSION

As pointed out in Sec. II, the DFWM measurements may give different values of $\chi^{(3)}$ if the relaxation parameters and the pulse width used in the experiment are not properly taken into account. We first discuss third-order susceptibilities in the case of the multiexponential time response before arguing the size dependence of the oscillator strength. As the laser pulse width used in our DFWM measurements is 20 ns, the slow components (the 30-ns and 400-ns components) in the decay curve for $R=4.0$ nm (Fig. 6) do not satisfy the cw excitation condition, i.e., $\tau_2, \tau_3 > t_p$.

When both transient and stationary processes are involved in the DFWM, we can derive a $\chi^{(3)}$ value defined for the stationary regime from the measured diffraction efficiency in the following way. The time-dependent scattering efficiency $\eta(t)$ measured in the vicinity of the resonance is expressed by[28,29]

$$\eta(t) \propto \Delta\alpha(t)^2 \propto [\sigma_{eff} N(t)]^2, \tag{8}$$

where $\Delta\alpha$ and σ_{eff} are the change of the absorption coefficient and the nonlinear absorption cross section, respectively, and $N(t)$ is the time-dependent carrier density. We use three decay components to describe $N(t)$ since the luminescence decay exhibits three-component decay behavior. By integrating the transient diffraction efficiency given by Eq. (8), we have the following equation, which relates the observed diffraction efficiency η_{obs} to the diffraction efficiency η_0 in the stationary regime:

$$\eta_{obs} = \frac{\eta_0}{(T_1^*)^2} \frac{1}{t_p} \int_0^{t_p} dt \left\{ \int_0^t dt' \, \frac{a\ \exp[-(t-t')/\tau_1] + b\ \exp[-(t-t')/\tau_2] + c\ \exp[-(t-t')/\tau_3]}{a+b+c} \right\}^2, \tag{9}$$

where the incident laser pulse is assumed to be a rectangular pulse with temporal duration of t_p. The first integral on t' from 0 to t describes the increase of $N(t)$ and the second integral on t from 0 to t_p accounts for the accumulation of diffraction signal detected within the laser pulse duration. The coefficients a, b, and c are the same as those used in Eq. (6). Using Eqs. (3) and (9), we can obtain the $\chi^{(3)}$ value in the stationary regime.

The transformation of an effective $\chi^{(3)}$ to a stationary $\chi^{(3)}$ based on Eqs. (3) and (9) was experimentally confirmed using CdS_xSe_{1-x} nanocrystals in glass for which measurements were done in the visible light region.[30] The transient DFWM signal measured by the three-beam boxcar configuration using a picosecond laser with a duration of 7 ps exhibits a two-component decay with time constants (relative intensity) of 400 ps (1) and 1000 ps (0.01) and the effective lifetime T_1^* is 406 ps. The diffraction efficiency η_{ps} measured using the 7-ps pulse laser is 5.2×10^{-9}, which is much smaller than $\eta_{ns}=2.3\times10^{-5}$ measured using the 7-ns pulse laser at the same excitation level of 10 kW/cm^2. If we use Eq. (3), the value of η_{ps} yields 2.3×10^{-8} esu for $|\chi_{ps}^{(3)}|$, while the value of η_{ns} yields 1.5×10^{-6} esu for $|\chi_{ns}^{(3)}|$. However, using Eqs. (3) and (9), we obtain $|\chi_{ps}^{(3)}|=2.3\times10^{-6}$ esu for η_{ps}. This value is in good agreement with the $\chi_{ns}^{(3)}$ value measured in the stationary regime within a factor 1.5. If we put directly η_{ps} and $T_1^*=406$ ps into Eq. (4), we can get the same value. Therefore, we can derive a stationary $\chi^{(3)}$ value that characterizes nonlinear properties of materials using Eqs. (3) and (9) even if there exists a multicomponent decay in the nonlinear time response. It is worthwhile to point out

that when we use a standard reference sample such as CS_2, response times of both the reference sample and the sample in the study must be much shorter than the pulse width used.[31] Only when the stationary grating in the DFWM configuration is generated for both of the samples do the measured diffraction efficiencies yield the stationary $\chi^{(3)}$ values. The $|\chi^{(3)}|$ values measured in this study were all calculated using Eq. (3) and were then compared with those calculated using Eqs. (3) and (9). However, the discrepancy was very small and the contribution of the slow components was found to be negligible. For example, in CuBr nanocrystals with $R=4.0$ nm, the decay kinetics is decomposed into three components and the slowest one is even longer than the pulse duration of 20 ns as shown in Fig. 6. The contributions of τ_1, τ_2, and τ_3 components estimated by using Eq. (9) were 91.3%, 8.2%, and 0.5%, respectively, and the slowest component of τ_3 was negligible.

We now discuss the size dependence of the oscillator strength derived from measurements of $|\chi^{(3)}|$, T_1^*, and Γ_h assuming the two-level system. As shown in Fig. 10, it is of interest to note that the size-dependent enhancement of f_x per nanocrystal does not saturate up to the largest size of $R\approx 34a_B$ studied here. This behavior is different from that observed in CuCl nanocrystals, where the decrease of oscillator strength is clearly observed for sizes larger than 5.0 nm.[17] In CuCl nanocrystals, the saturation of the size enhancement was argued in terms of the following mechanisms.[17] First, the energy splitting of the confined levels in large nanocrystals becomes smaller and higher confined levels are thermally excited. The thermal energy k_BT corresponds to the confinement energy ΔE for the nanocrystals for which f_x has a maximum value. The oscillator strength is then redistributed among the thermally activated sublevels, which leads to the decrease of f_x defined for the two-level system. Second, when the longitudinal-transverse splitting Δ_{LT} becomes comparable to the confinement energy, the giant-oscillator-strength effect disappears. The unsaturated behavior of f_x observed in CuBr nanocrystals may be explained by both of the mechanisms because both conditions ΔE ($\geqslant$21 meV) $>k_BT$ (6.7 meV for 77 K) and ΔE ($\geqslant$21 meV)$>\Delta_{LT}$ (12.5 meV) are satisfied for all the samples studied here. If we consider the Γ_8 valence band of CuBr consisting of the light and heavy hole, the multicomponent exciton state may be responsible for the unsaturated behavior. Nair and Takagahara took into account a two-exciton state (biexciton) that has a giant oscillator strength in large CuCl quantum dots.[32] A pronounced cancellation of contributions to $\chi^{(3)}$ occurs between the two-exciton state and the lowest exciton state, which results in the saturation behavior in CuCl nanocrystals. On the other hand, such a cancellation may be complicated in CuBr nanocrystals probably due to the multicomponent nature of the lowest Z_{12} excitons and the corresponding two-exciton states.[33] This is still an open question to be answered; further study is going on using nanocrystals consisting of the solid solution of CuBr and CuCl in which the band structure changes with composition.

It is worth noting that the nonlocal effect does not work in the crystallite sizes studied here. The light wavelength λ_m near the resonance of Z_{12} excitons in the 40-nm nanocrystal is estimated from the dispersion relation of the dielectric constant. Taking $E_T=2.981$ eV and $\Gamma_h=4.0$ meV, the refractive index near the resonance is calculated to be 4.03, which yields $\lambda_m\sim 100$ nm. The largest size of the CuBr nanocrystal in this study is still smaller than the limit where the long-wavelength approximation fails to hold. The nonlocal effects might be important in the size range $R\geqslant 100$ nm.[14]

The magnitude of the giant oscillator strength is compared to that of the oscillator strength of bulk excitons. The value of f_x is estimated using[17]

$$\text{Im}\ \chi^{(3)}=1.3\times 10^{17}\times\left[\frac{n}{(n^2+2)^2}\right]\left(\frac{e^2}{2m_0\omega}\right)^2\hbar f_x\frac{\alpha T_1}{\Gamma_h}. \tag{10}$$

Taking the value of 1.2×10^{-4} esu eV cm/s as $|\chi^{(3)}|\Gamma_h/\alpha T_1^*$ for $R=2.7$ nm and 8.3×10^{-2} esu eV cm/s for $R=42$ nm, we estimate 0.036 and 24, respectively. Comparing to the oscillator strength per unit cell in the bulk CuBr, which is $f_{Z12}=0.014$, the enhancement factor f_x/f_{Z12} turns out to be 1.7×10^3 for $R=42$ nm, which is of the same order of magnitude as that for CuCl nanocrystals.[17]

Finally, we discuss the size dependence of $\chi^{(3)}$ in nanocrystals and quantum-well (QW) structures. For simplicity, let us consider the case of the constant volume fraction r of nanocrystals in glass, i.e., $N=3r/4\pi R^3$ in Eq. (1), and assume that T_1 and Γ_h are size independent. In the weak-confinement regime ($R/a_B\gg 1$) the observed dependence of f_x is $R^{2.0}$, whereas the theoretical dependence is R^3 for the infinite potential.[5,11] Therefore, $\chi^{(3)}$ exhibits the size dependence of R^1 and R^3 for $f_x\propto R^2$ and R^3, respectively. This enhancement of $\chi^{(3)}$ with *increasing* dimension in the weak-confinement regime essentially originates from the size-dependent enhancement of oscillator strength per nanocrystal, which results from the coherent superposition of the dipole moment within the envelope function of exciton. In the strong-confinement regime ($R/a_B\ll 1$), on the other hand, f_x is approximately independent of R.[5] Then Eq. (1) gives the R^{-3} dependence of $\chi^{(3)}$. The enhancement of nonlinearity with *decreasing* size in the strong-confinement regime results from the increase of nanocrystal density under the condition of the constant volume fraction. This enhancement can be compared to the well-width dependent enhancement of $\chi^{(3)}$ in QW structures. In typical QW structures of III-V semiconductors, the well width l_z is smaller than a_B and the exciton oscillator strength *per unit surface* is proportional to $1/\pi a_B^2$. In the exact two-dimensional limit, the Bohr radius is reduced to $a_B/4$.[34] The theoretical calculation of $\chi^{(3)}$ shows the l_z^{-1} dependence if we ignore the well-width dependence of T_1 and Γ_h.[35] Therefore, the nonlinearity in QW structures is enhanced with *decreasing* dimension, which is in contrast to the case of nanocrystals in the weak-confinement regime.

V. CONCLUSION

We have investigated the size-dependent optical nonlinearity in CuBr nanocrystals over the wide range of sizes by means of DFWM, luminescence lifetime, and resonant luminescence experiments. The measurements of the dispersion of $|\chi^{(3)}|$ reveal that the nonlinearity is governed by resonant

enhancement of confined excitons. The figure of merit $|\chi^{(3)}|/\alpha$ at the resonance with Z_{12} excitons exhibits the size-dependent enhancement. The measured lifetime and homogeneous width show the size dependences of $R^{-1.5}$ and $R^{0.1}$, respectively. The size dependence of the oscillator strength of Z_{12} excitons was derived from the measured relaxation parameters. An unambiguous size enhancement of the oscillator strength per nanocrystal was elucidated in CuBr nanocrystals, i.e., $f_x \propto R^{2.0}$ for $2.7 \leqslant R \leqslant 42$ nm. The giant oscillator strength exhibits the enhancement by the factor of 2.6 to 1.7×10^3 depending on the crystallite radius from 2.7 nm to 42 nm. The size dependence of oscillator strength does not exhibit the saturation behavior for the larger sizes, which is unlike the case of CuCl nanocrystals. This result suggests an important role of the valence-band structure in the size-dependent enhancement of nonlinear polarization in the resonant regime. We have also pointed out that DFWM measurements in the transient regime yield an effective $\chi^{(3)}$, which is dependent on the pulse duration used in the measurement, and the effective $\chi^{(3)}$ can be transformed to the stationary $\chi^{(3)}$ by the formula that takes into account the transiently generated nonlinear grating in the sample. To characterize the third-order nonlinearity of nonlinear materials, it is better to use a stationary $\chi^{(3)}$ that is independent of the experimental parameters.

ACKNOWLEDGMENTS

The authors thank T. Manabe and N. Sugimoto at Asahi Glass Co., Ltd. for preparing CuBr-doped glasses and N. Sakabe, A. Nakagawa, N. Watanabe, S. Adachi, and S. Ikemizu for their experimental help at Photon Factory. The authors are also grateful to M. Sakata, T. Takagahara, T. Tokizaki, and M. Ichida for helpful discussions. Y.L. thanks Aichi Science & Technology Foundation for financial support. This work was supported by a Grant-in-Aid for Scientific Research from the Ministry of Education, Science and Culture of Japan, the New Energy and Industrial Technology Development Organization, the Asahi Glass Foundation, and the Aichi Science & Technology Foundation.

*Present address: Faculty of Science and Engineering, Shimane University, Matsue 690, Japan.

[1] See, for example, *Optical Nonlinearities and Instabilities in Semiconductors*, edited by H. Haug (Academic, San Diego, 1988).
[2] R. K. Jain and R. C. Lind, J. Opt. Soc. Am. **73**, 647 (1983).
[3] A. L. Efros and A. L. Efros, Sov. Phys. Semicond. **16**, 772 (1982).
[4] L. E. Brus, J. Chem. Phys. **80**, 4403 (1984).
[5] Y. Kayanuma, Phys. Rev. B **38**, 9797 (1988).
[6] S. Schmitt-Rink, D. A. B. Miller, and D. S. Chemla, Phys. Rev. B **35**, 8113 (1987).
[7] P. Roussignol, D. Ricard, and C. Flytzanis, Appl. Phys. B: Photophys. Laser Chem. **51**, 437 (1990).
[8] D. W. Hall and N. F. Borrelli, J. Opt. Soc. Am. B **5**, 1650 (1988).
[9] S. H. Park, R. A. Morgan, Y. Z. Hu, M. Linderberg, S. W. Koch, and N. Peyghambarian, J. Opt. Soc. Am. B **7**, 2097 (1990).
[10] H. Shinojima, J. Yumoto, and N. Uesugi, Appl. Phys. Lett. **60**, 298 (1992).
[11] E. Hanamura, Phys. Rev. B **37**, 1273 (1988).
[12] T. Takagahara, Phys. Rev. B **39**, 10 206 (1989).
[13] F. C. Spano and S. Mukamel, Phys. Rev. A **40**, 5783 (1989).
[14] H. Ishihara and K. Cho, Phys. Rev. B **42**, 1724 (1990).
[15] Y. Masumoto, M. Yamazaki, and H. Sugawara, Appl. Phys. Lett. **53**, 1527 (1988).
[16] B. L. Justus, M. E. Seaver, J. A. Ruller, and A. J. Campillo, Appl. Phys. Lett. **57**, 1381 (1990).
[17] T. Kataoka, T. Tokizaki, and A. Nakamura, Phys. Rev. B **48**, 2815 (1993).
[18] U. Woggon, F. Henneberger, and M. Muller, Phys. Status Solidi B **150**, 641 (1988).
[19] R. Kippelen, R. Levy, P. Faller, P. Gilliot, and l. Belleguie, Appl. Phys. Lett. **59**, 3378 (1991).
[20] A. Nakamura, H. Yamada, and T. Tokizaki, Phys. Rev. B **40**, 8585 (1989).
[21] T. Itoh, M. Furumiya, and C. Gourdon, Solid State Commun. **73**, 271 (1990).
[22] A. Nakamura, Y. Li, T. Kataoka, and T. Tokizaki, J. Lumin. **60&61**, 376 (1994).
[23] Y. Kondo, N. Sugimoto, T. Manabe, S. Ito, T. Tokizaki, and A. Nakamura, Nonlinear Opt. **13**, 143 (1995).
[24] P. N. Butcher, and D. Cotter, *The Elements of Nonlinear Optics* (Cambridge University Press, Cambridge, 1990).
[25] T. Itoh and M. Furumiya, J. Lumin. **48&49**, 704 (1991).
[26] T. Wamura, Y. Masumoto, and T. Kawamura, Appl. Phys. Lett. **59**, 1758 (1991).
[27] T. Tokizaki, T. Kanetaka, H. Ohmura, and A. Nakamura, Prog. Cryst. Growth Charact. Mater. **33**, 187 (1996).
[28] D. S. Chemla, D. A. Miller, P. W. Smith, A. C. Gossard, and W. Wiegmann, IEEE J. Quantum Electron. **20**, 265 (1984).
[29] M. N. Islam, E. P. Ippen, E. G. Burkhardt, and T. J. Bridges, J. Appl. Phys. **59**, 2619 (1986).
[30] H. Hiraga, S. Ohmi, T. Tokizaki, and A. Nakamura (unpublished).
[31] B. P. Singh, M. Samoc, H. S. Nalwa, and P. N. Prasad, J. Chem. Phys. **92**, 2756 (1990).
[32] S. V. Nair and T. Takagahara, Phys. Rev. B **53**, R10 516 (1996).
[33] T. Takagahara (private communication).
[34] M. Shinada and S. Sugano, J. Phys. Soc. Jpn. **21**, 1936 (1966).
[35] M. Kumagai and T. Takagahara, Phys. Rev. B **40**, 12 359 (1989).